IEEE Photonics Journal
An IEEE Photonics Society Publication

Open Access

Si_3N_4-Based Integrated Optical Analog Signal Processor and Its Application in RF Photonic Frontend

Volume 7, Number 5, October 2015

Hongchen Yu, Student Member, IEEE
Minghua Chen, Member, IEEE
Qiang Guo
Marcel Hoekman
Hongwei Chen, Member, IEEE
Arne Leinse
Rene G. Heideman
Richard Mateman
Sigang Yang, Member, IEEE
Shizhong Xie, Senior Member, IEEE

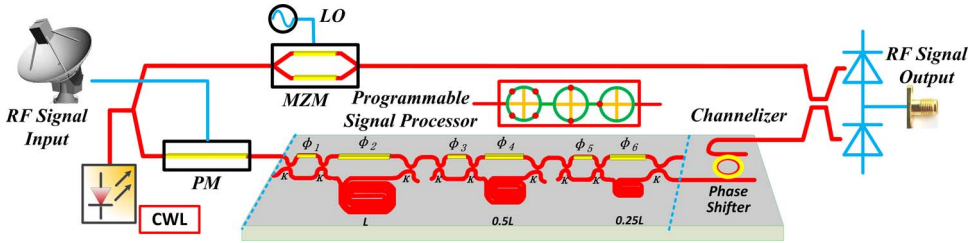

DOI: 10.1109/JPHOT.2015.2471084
1943-0655 © 2015 IEEE

IEEE photonics SOCIETY

IEEE

Si_3N_4-Based Integrated Optical Analog Signal Processor and Its Application in RF Photonic Frontend

Hongchen Yu,[1,2] *Student Member, IEEE*, Minghua Chen,[1,2] *Member, IEEE*, Qiang Guo,[1,2] Marcel Hoekman,[3] Hongwei Chen,[1,2] *Member, IEEE*, Arne Leinse,[3] Rene G. Heideman,[3] Richard Mateman,[3] Sigang Yang,[1,2] *Member, IEEE*, and Shizhong Xie,[1,2] *Senior Member, IEEE*

[1]Tsinghua National Laboratory for Information Science and Technology, Beijing 100084, China
[2]Department of Electronic Engineering, Tsinghua University, Beijing 100084, China
[3]LioniX, 7500 AL Enschede, The Netherlands

DOI: 10.1109/JPHOT.2015.2471084

Manuscript received June 3, 2015; revised August 17, 2015; accepted August 18, 2015. Date of publication August 20, 2015; date of current version September 2, 2015. This work was supported in part by the National Program on Key Basic Research Project (973) under Contract 2012CB315703; by the National Science Foundation of China under Contract 61335002, Contract 61120106001, Contract 61271134, Contract 61322113; by the Program for New Century Excellent Talents in University under Grant NCET-10-0520; and by the Tsinghua University Initiative Scientific Research Program. Corresponding author: M. Chen (e-mail: chenmh@tsinghua.edu.cn).

Abstract: Digital signal processing has achieved great success in the field of signal processing over the past several decades. However, as the bandwidth requirement increases, the power consumption and effective number of bits (ENOB) of the analog-to-digital convertor (ADC) have become bottlenecks. One solution is returning to analog and applying microwave photonic technologies, which shows potential for multiband signal processing. In this paper, a programmable integrated analog photonic signal processor based on cascaded Mach–Zehnder interferometers (MZIs) and a channelized filter has been proposed. Different shapes of the signal processor can be acquired for different applications. The highest processing resolution is 143 MHz, and the processing range of the signal processor can be higher than 112.5 GHz. An application of the signal processor for the signal extraction in a radio frequency (RF) photonic frontend operating from L-band to K-band is presented.

Index Terms: Integrated optics devices, radio frequency (RF) photonics, analog optical signal processing.

1. Introduction

Signal processing has become increasingly important for its potential applications in science and engineering, which generally contains two subfields: analog signal processing and digital signal processing. Since the development of digital signal processing in the 1960s, signal processing in the field of radio frequency (RF) wireless communication [1], [2] or optical communication [3], [4] has been mostly transformed from the analog to digital domain. This allows for many advantages like for instance flexible programmable signal processing, high stability and interference tolerance. In particular, software radio (SR) technologies have been more inspired to researchers in RF receivers since 1990s for their potential advantages of flexibility and reconfiguration [5]–[7].

With the explosive development of wireless communication, radar communication, etc., the bandwidth requirement of the system to analog-to-digital converters (ADCs) or digital signal processors (DSPs) has grown to be higher than 10 GHz. However, achieving low power consumption at such high frequencies with an acceptable effective number of bits (ENOB) is not feasible nowadays [8]–[10]. One of the potential methods based on analog pre-signal processing has been proposed to compensate the weakness of the digital methods [11], [12], whose aim is to simplify the analog input signal to the ADC/DSP, thus decrease the bandwidth and power consumption requirement of the ADC/DSP to an acceptable range. Nevertheless, it is inherently difficult for electrical methods to implement a flexible tunable broadband scheme. Microwave photonics combines the RF and photonics, which can overcome the bandwidth limitations of the electrical domain and dramatically decrease power consumption at the same time [13]–[15], thanks to the advantages of parallelism processing, large bandwidth, low loss, flexible tunability, and immunity to electromagnetic interference (EMI) [16], [17]. The microwave photonic signal processors have been extensively researched and some meaningful efforts have been raised, especially the integrated ones are more attractive because of its small size and robustness [18]. In [19] and [20], Telcordia's researchers proposed a programmable signal processor with a resolution (3-dB bandwidth) of nearly 1–2 GHz. In [21], a cascaded lattice based signal processor with four zeros and poles is presented. In [22], a signal processor in InP-InGaAsP platform has been proposed with a tunable bandwidth of larger than 1.9 GHz. In our previous work, a silicon-on-insulator (SOI) Mach–Zehnder interferometers (MZIs)-based signal processor has been proposed with a resolution of approximately 1.536 GHz [23]. However, for nowadays and the near future communication applications, the effective bandwidth of the desired signal is usually around 100 MHz [24], [25], even if at higher carrier frequency. There is a gap of approximately one order of magnitude between the resolutions of the proposed signal processors and the bandwidth of the desired signal, which are partially limited by the high waveguide loss of the waveguide. Our co-authors from LioniX B.V. demonstrated a Si3N4 waveguide with an ultralow waveguide loss of 0.1 dB/cm at the bend radius of 70 μm [26]–[28], which shows potential for longer delays and higher resolution signal processors.

In this work, a seven-zeros programmable analog signal processor based on Si_3N_4 waveguides has been proposed and experimentally demonstrated. The amplitude and the phase of the zeros can be tuned to achieve different response shapes. The highest resolution and processing range of the signal processor are less than 143 MHz and larger than 112.5 GHz, respectively, which make it feasible for multi-band microwave signal processing.

2. Device Design and Simulation

In our previous work [23], limited by the high SOI waveguide loss of about 3 dB/cm, only a 3-cm long delay has been fabricated to obtain a filter with a resolution of approximately 1.5 GHz, which is not enough for the application of wireless communication nowadays. Our co-authors from LioniX B.V. proposed a Si_3N_4 waveguide possessing an ultralow waveguide loss of 0.1 dB/cm at the bend radius of 70 μm [26]–[28], which provides the possibility to realize a long delay to get sub-MHz resolution for the signal processor and a high-Q ring resonator for the channelized filter with large processing range.

Based on this low loss waveguide, we propose a novel programmable bandpass filter-based RF photonic frontend as shown in Fig. 1. The down-conversion and optical filtering are combined to simplify the signal and down-convert the desired signal to baseband or intermediate frequency (IF) band before sending it to the ADC/DSP, which can decrease the bandwidth and power consumption requirement to an acceptable range. The signal processor system in this frontend includes the programmable signal processor based on the cascaded MZIs and the channelized filter based on the add-drop ring resonator. In the programmable filter, three tunable couplers based on single stage MZI with identical arm lengths and two 50:50 couplers [29] are adopted to balance the input power to the two arms of each of the three stage asymmetric MZIs. The coupling ratios of the directional couplers utilized in this design are all 50:50 so that

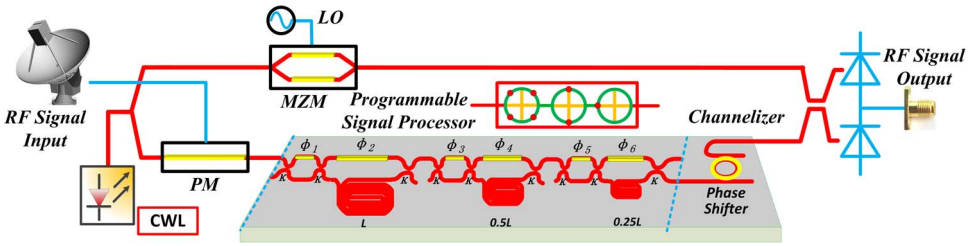

Fig. 1. Schematic diagram of the RF photonic frontend based on the programmable signal processor. The upper path is for the LO, and the lower path is for the RF signal. The RF signal is up-converted to the optical domain with a phase modulator (PM) and processed by the programmable signal processor, which includes three tunable couplers based on the identical MZI and three stage asymmetric MZIs. A channelized filter based on the ring resonator is introduced to enhance the processing range of the signal processor. The LO and the filtered signal combine at a 50:50 coupler and are detected by a BPD to obtain the desired signal in baseband or IF frequency band.

the coupling ratio of the tunable coupler can be tuned from 0 to 1 in theory. The differential path length of the first asymmetric MZI is the largest length L, the second stage is L/2, and the third stage is L/4. On top of one arm of the MZIs are the phase shifters, which can be used to tune the coupling ratio and adjust the phase relationship among the three stage asymmetric MZIs.

The simulation of the device is performed by the transfer matrix method [29], which can derive the transfer function of the filter system, and with the help of Matlab, the device performance can be simulated at different parameters. The transfer function of the proposed filter is derived by the transfer matrix methods as shown in

$$T = \left[r(r^2e^{-j\varphi_1} - t^2)e^{-j\varphi_2} - t^2re^{-j\beta L}\gamma_1(e^{-j\varphi_1} + 1)\right]\left[r(r^2e^{-j\varphi_3} - t^2)e^{-j\varphi_4} - t^2re^{-j\beta L/2}\gamma_2(e^{-j\varphi_3} + 1)\right] * \left[r(r^2e^{-j\varphi_5} - t^2)e^{-j\varphi_6} - t^2re^{-j\beta L/4}\gamma_3(e^{-j\varphi_5} + 1)\right] \quad (1)$$

where $r = \sqrt{1-\kappa}$, $t = \sqrt{\kappa}$, κ is the amplitude coupling ratio of the couplers. φ_i is the phase introduced by the phase-shifters, $\beta = 2\pi n_{eff}/\lambda$, n_{eff} is 1.535, the effective refractive index of the waveguide, λ is the wavelength of the light, and γ_i is the amplitude loss difference induced by the differential path length of the MZIs. The coupling ratios of the direct couplers utilized in this design are all 50:50, so the transfer function can be simplified to

$$T = \frac{\sqrt{2}}{32}\left[(e^{-j\varphi_1} - 1)e^{j\varphi_2} - e^{-j\beta L}\gamma_1(e^{-j\varphi_1} + 1)\right]^*\left[(e^{-j\varphi_3} - 1)e^{j\varphi_4} - e^{-j\beta L/2}\gamma_2(e^{-j\varphi_3} + 1)\right] * \left[(e^{-j\varphi_5} - 1)e^{j\varphi_6} - e^{-j\beta L/4}\gamma_3(e^{-j\varphi_5} + 1)\right], \quad (2)$$

The phase on one arm of the MZIs φ_i can be tuned by the phase shifter on top of the waveguides. In theory, the coupling ratio of the tunable coupler can be tuned from 0 to 1 by tuning the phase $\varphi_{1,3,5}$, when the coupling ratios of the two directional couplers are all 50:50 exactly.

Seen from the direct form implementation of the proposed programmable 7-zeros FIR filter in Fig. 2(a), the amplitude and phase of the first four-zeros are coupled and fully decided by the power ratio ($\cos(\alpha_1)$ and $\sin(\alpha_1)$) of the first tunable coupler and the phase φ_2. There is a $\pi/2$ phase difference between the four-zeros, as shown in green in Fig. 2(b)–(d). The second two-zeros are coupled and decided by the power ratio ($\cos(\alpha_2)$ and $\sin(\alpha_2)$) of the second tunable coupler and phase α_4. There is a π phase difference between the two-zeros, as shown in yellow. The third one-zero is determined by the power ratio ($\cos(\alpha_3)$ and $\sin(\alpha_3)$) of the third tunable coupler and the phase φ_6, as the one-red zero shows. By tuning the phase φ_i, the amplitude and the phase of the seven-zeros can be altered, i.e. the shape of the filter can be varied. Because of the characteristic of the MZIs-based filter, the FSR of the filter is usually limited to approximately two times of the 3 dB-bandwidth, which would limit its application. In this

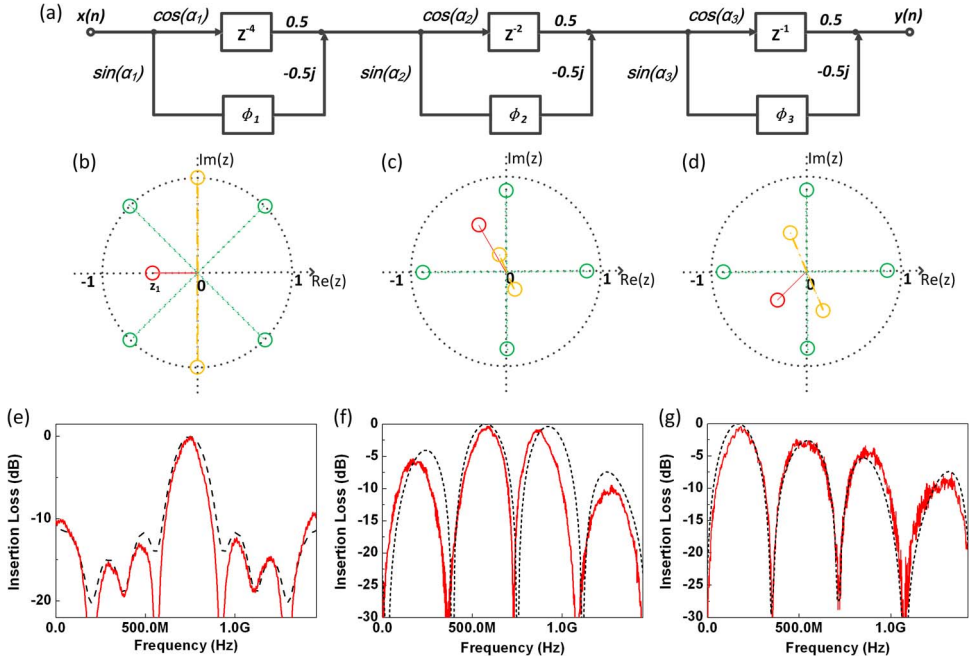

Fig. 2. Device principle and performance. (a) Direct form implementation of the 7-zeros FIR filter. $\cos(\alpha_i)$ and $\sin(\alpha_i)$ are the power distribution ratios to the two-arms of the MZIs. Characterized responses of the reconfigurable signal processor at different zeros distribution. (b)–(d) The four different zeros distribution. (e)–(g) The response of the signal processor relative to the zeros-distribution in (b)–(d). The solid red lines are the experimental measured response, and the dashed lines are simulated.

design, 3-stage cascaded MZIs are employed to achieve a four times enhancement in FSR. To further enhance the FSR, a channelized filter based on the microring resonator bandpass filter is implemented as shown in Fig. 1. Thanks to the index-contrast between the SiO_2 and the Si_3N_4 and the low waveguide loss, the ultra-high Q filter with a large FSR tends to be realized as a channelized filter.

3. Fabrication and Device Test

The proposed fully-reconfigurable high resolution FIR signal processor is fabricated by the Si_3N_4 technology as the picture of the device shows in Fig. 3(a). The waveguide is constructed by two 170 nm strip Si_3N_4 waveguides in high refractive index, which is separated by a 500 nm SiO_2 layer in the middle [27]. The width of the waveguide is 1.2 um. The loss of this double-strip Si_3N_4 waveguide is typically lower than 0.1 dB/cm @ 70 μm radius. To achieve a FIR filter with a 3 dB-bandwidth of around 100 MHz, the largest delay L in this structure is set to 50 cm, which would cause a loss difference between the two arms of the MZI. The differential path length of the second and third stage MZIs are 25 cm and 12.5 cm, respectively, which would also induce loss difference between two arms of each MZI. The tunable couplers based on the identical arm length MZI are introduced to balance the power distribution to the unbalanced two-arms of the MZI to optimize the filtering response with a tuning speed of approximately 500 μs. The resistances of the Cr/Au heater on top of one MZI arm are around 300 Ω, separated by the cladding layer of an 8 μm thick thermal oxide. The radius and gap between straight waveguides and microring of the add-drop microring resonator for the channelized filter are 125 μm and 2 μm, respectively.

A tunable high-resolution optical network analyzer based on the RF vector network analyzer (VNA) is designed to measure the response of the filter as presented in Fig. 3(a). In this system, a tunable laser source is separated to two paths with a 50:50 coupler, where one is used as the

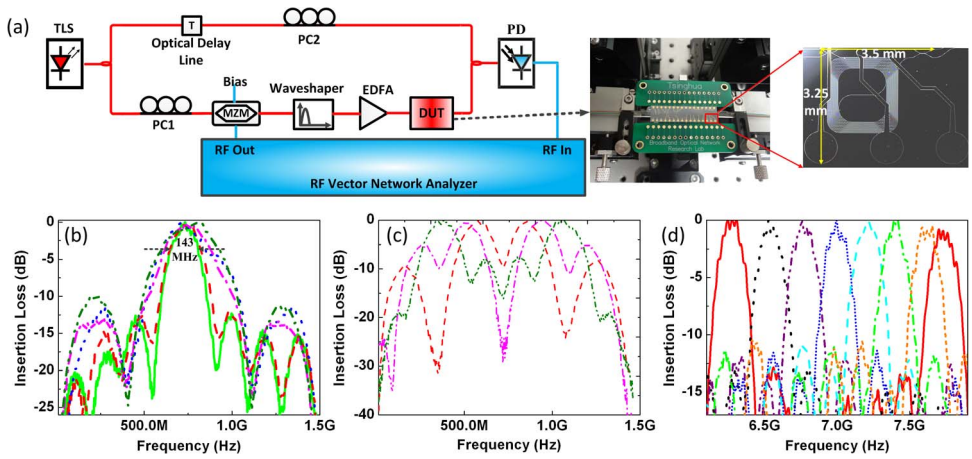

Fig. 3. Device measurement with VNA. (a). A VNA-based high resolution optical vector network analyzer for measuring the performance of the high resolution reconfigurable signal processor. (Right) Packaging of the chip and the picture of the last stage MZI. The response of the programmable signal processor. (b) Signal-band response with bandwidth variation from 143 MHz to 300 MHz of a single bandpass response. (c) Dual-band response with different separation. (d) Center frequency variation of the single bandpass response.

optical local oscillator (LO) for down-converting, and the other is used as the optical carrier for up-converting the RF sweeping source from the VNA to optical domain by the MZM to be an optical sweeping source with the same sweeping resolution of the RF VNA. The null-biased MZM is adopted to achieve the carrier-suppressed modulation of the RF sweeping source, and as the response of the filter is periodic, a single bandpass filter is introduced to filter out the positive modulated bands to avoid the interference of the negative modulated sidebands to be the clean optical sweeping source. Then, an erbium doped fiber amplifier (EDFA) is introduced to amplify the optical sweeping source before being sent into the device-under-test (DUT). As the device is polarization sensitive, a polarization controller (PC) is set before the device to tune the polarization to get the optimized coupling ratio. After that, the modulated bands are filtered by the proposed filter. Then, the filtered signal is combined with the LO, detected by a photodetector to the electronic domain, and sent back to the RF VNA to get the filter's response. Because of the size mismatching between the waveguide and the optical fiber, the spot size convertors provided by the LioniX B.V. are utilized to lower the coupling loss to around 3.5 dB. The measured fiber-to-fiber loss is about 20 dB, and therefore, the device loss is about 13 dB.

In our experiment, with properly tuning the phase on one arm of the MZIs, different shapes of response have been achieved. For example, in a single FSR, filters with 1 passband, 2 passbands and 4 passbands can be realized and the measured results agree well with simulation results as shown in Fig. 2(e)–(g), when the zeros are distributed as presented in Fig. 2(b)–(d). The device parameters are listed as $L = 0.5$ m and $n = 1.99$.

For the application of signal extraction, such as in wireless communications [24], [25], the single passband and dual-band filter have been realized as shown in Fig. 3(b) and (c). The resolution of the filter can be altered from 143 MHz to more than 300 MHz with properly tuning the phase shifters on top of the MZIs as presented in Fig. 3(b) and the FSR of the filter is maintained at approximately 1.466 GHz, which is enhanced by the scheme of cascaded MZIs as described in [23]. As can be seen in Fig. 3(c), for the dual-band filter, the interval between the two passbands can be altered without changing the 3-dB bandwidth of the two passbands, by tuning the phase shifters on top of the filter, and the center frequency of the filter can also be swept with the thermoelectric cooler (TEC) module, as shown in Fig. 3(d). The 3 dB-bandwidth and the FSR of the channelized filter in this design are approximately 420 MHz and 225 GHz, respectively, which can extend the operating frequency range of the signal processor from the L-band to W-band.

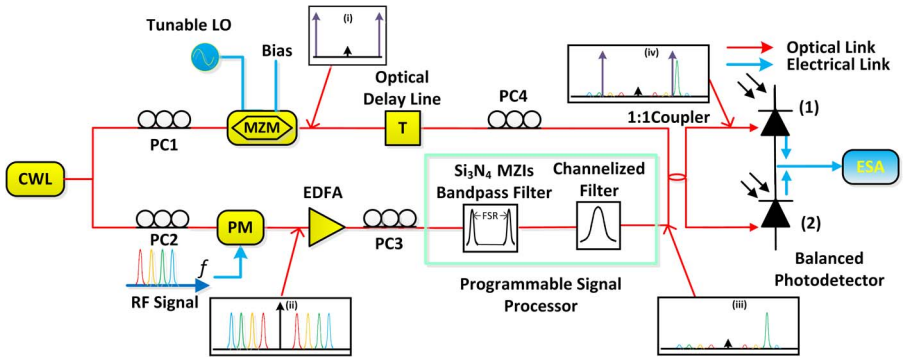

Fig. 4. Schematic diagram of the RF photonic frontend. The LO and RF signal are up-converted to optical domain with the MZM and PM, respectively. The desired signal is extracted by the proposed programmable signal processor with a cascading channelized filter. The BPD used in this system can suppress the even-order nonlinear signal and provide additional gain.

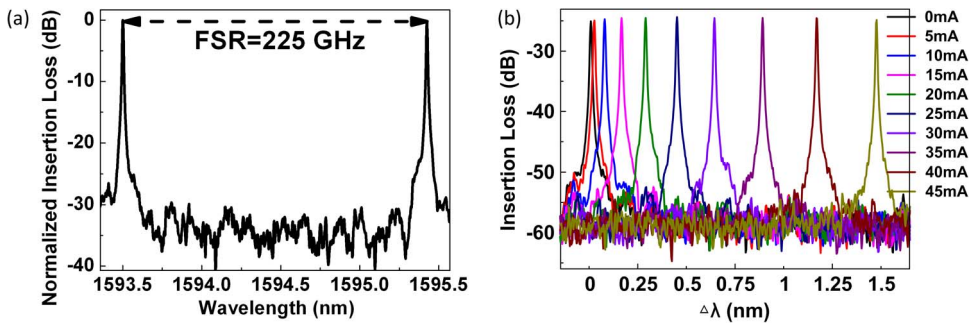

Fig. 5. Transfer response of the channelized filter. (a) Transfer response of the channelized filter measured by the OVA. (b) The thermal tuning response of the filter for 1 FSR.

4. Experimental Section

In the experiment, a multi-band RF photonic frontend based on the proposed single passband filter is performed as the experimental setup shown in Fig. 4, which is introduced to evaluate the performance of the signal processor. In this frontend, a continuous wave laser (CWL) is divided to two paths by a 50:50 coupler and serves as the carriers for the LO and signal. The LO is up-converted to optical domain by a null-biased MZM to achieve a carrier-suppressed modulation, which is used as the optical LO for down-converting. The lower path is used as the optical carrier for phase-modulation of the received signal. As the electro-optical (EO) modulators are polarization-sensitive, the PCs are put before them to achieve the optimized modulation efficiency. An EDFA is utilized to amplify the signal before being sent into the signal processor for signal extraction. Then the extracted signal would be coupled with the LO at a 50:50 coupler and detected by a balanced photodetector (BPD) to get the desired signal for users. As the devices are all polarization sensitive, a PC is set to maintain the TE polarization and achieve a smaller coupling loss. In this experimental setup, a channelized filter based on the micro ring resonator is introduced to enhance the processing range and outside band suppression ratio of the signal processor and the performance of the filter is measured by the OVA (LUNA) as presented in Fig. 5. The 3 dB-bandwidth, the FSR, and the outside band suppression ratio of the filter are approximately 420 MHz, 225 GHz, and 42 dB, respectively [30]. The insertion loss of the channelized filter is approximately 9 dB including the fiber coupling loss. The center frequency of the channelized filter can be altered by more than 1 FSR with current lower than 45 mA, as given in Fig. 5(b), with a resistance of about 200 Ω. Thanks to the narrow bandwidth and high out of band suppression ratio

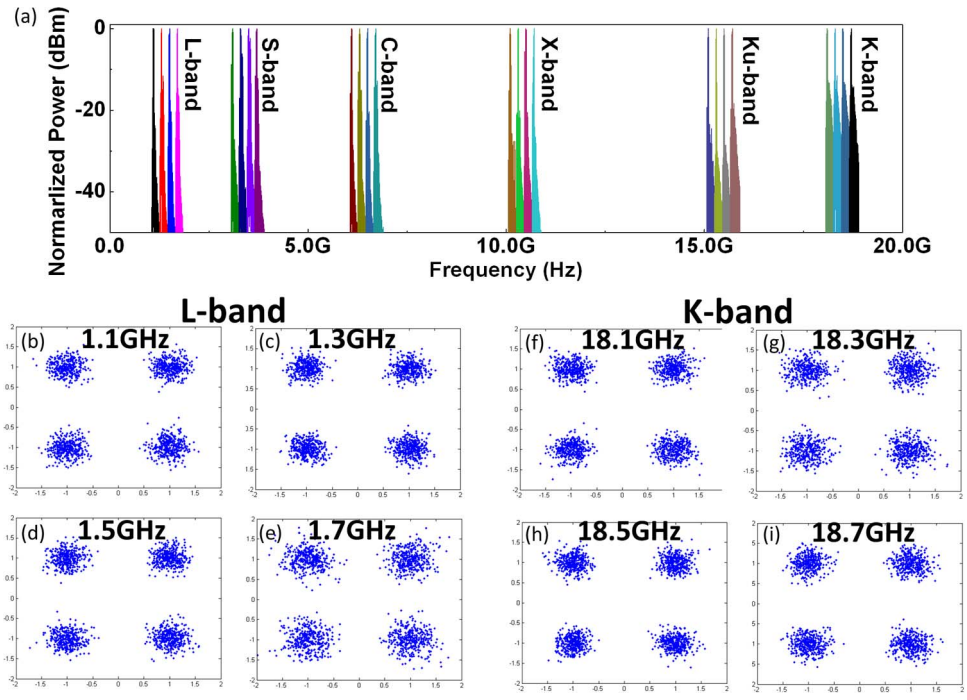

Fig. 6. Experiment results. (a) The four-band bandwidth signal with a bandwidth of about 20 MHz extracted by the proposed bandpass high-resolution signal processor from L- to K-band. (b)–(e) Constellations of the recovered four-band bandwidth signal in L-band. (f)–(i) Constellations of the recovered four-band bandwidth signal in the K-band.

of the channelized filter, the out of band noise induced by the EDFA can also be suppressed effectively so that the intensity noise impact on the transmitted signal would be reduced.

The parameters of the system are listed as follows, the center wavelength and the output power of the continuous wave laser (CWL) are 1549.407 nm and 16.96 dBm, respectively and the bandwidth of the MZM is 40 GHz. The bandwidth and half-wave voltage of the phase modulator (PM) are 40 GHz and 7 V, respectively and the injected signals in the experiment are produced by the arbitrary waveform generator (AWG, Tektronix), the gain of the EDFA is approximately 10 dB to compensate the loss of the whole link, the BPD used in this system is the Thorlabs PDB410C with a responsivity of approximately 1.0 A/W.

To investigate the performance of the proposed programmable signal processor, multi-band (from the L-band to the K-band) signals are generated as the test signal for signal extraction. As long as the entire signal bandwidth is smaller than half of the FSR of the channelized filter, and each bandwidth of the signal is smaller than the bandwidth of the programmable signal processor, the desired signal would be extracted out by the filter, by simply tuning the center frequency of the filter to the center of the desired signal. In the experiment, the four-band signal with a 20 MHz bandwidth each and a separation of about 200 MHz is generated to represent the signal in wireless communications, such as the Wi-Fi signal. The modulation format of the OFDM signals is 4-QAM with 1000 carriers. The detail of the used 4-QAM OFDM signal is listed as follows: the FFT size is 100000, the length of the cyclic prefix is 10, the number of the training symbol is 2, and the real date rate is 40Mbps. As an example, the four-band signal at the frequency bands, L-band (1.1, 1.3, 1.5, and 1.7 GHz), S-band (3.1, 3.3, 3.5, and 3.7 GHz), C-band (6.1, 6.3, 6.5, and 6.7 GHz), X-band (10.1, 10.3, 10.5, and 10.7 GHz), Ku-band (15.1, 15.3, 15.5, and 15.7 GHz) and K-band (18.1, 18.3, 18.5, and 18.7 GHz) are injected to the phase-modulator for signal extraction in this experiment. By tuning the center frequency of the filter, the desired-band signal would be extracted. By tuning the frequency of the LO, the center frequency of the down-converted signal can be maintained at 40 MHz and the filtered signal is detected by the

100 MHz BPD to get the down-converted signal. The filtered four-band signals at different frequency bands are shown in Fig. 6(a). As can be seen in Fig. 6(a), all the signals at different frequency band range from the L-band to the K-band are well extracted by the proposed filter and recovered. The constellation of the received four band signals at the L-band and the K-band are shown in Fig. 6(b)–(i) as an example and the EVM in L-band and K-band are around 18% and 17.6%, respectively. The signal-to-noise ratios (SNRs) in the L-band and K-band are approximately 11.9 dB and 12.5 dB, respectively. Limited by the effective bandwidth of the AWG and the lowest frequency output of the microwave source, only the signals at L-to K-band are injected to this system to test the performance of the proposed signal processor.

The electrical power consumption of the device in the experiment is about 0.52 W, which includes two parts, tuning the zeros of the signal processor to achieve a 143 MHz bandwidth of about 0.12 W and altering the center frequency of the channelized filter in the entire FSR of around 0.4 W.

Employing such a programmable signal processor-based RF photonic frontend, the RF bandwidth signals from the L-band to the K-band are extracted by the signal processor and down-converted to IF band below 100 MHz, which decreases the bandwidth requirement of the ADC, i.e., decreases the power consumption and increases the ENOB effectively.

5. Conclusion

In this paper, a programmable high resolution and large processing range signal processor has been proposed and experimentally demonstrated, based on the cascaded MZIs and the ring resonator. Seven-zeros of the MZIs filter can be separated to three-parts for separately tuning the phase-shifters on the structure. Namely, the shape of the signal processor can be altered, which can be applied to reshape the signals to compensate system non-uniformities. With the help of the ultralow loss Si_3N_4 waveguide, a delay line as large as 50 cm has been fabricated and the highest resolution of the proposed signal processor measured in our experiment is about 143 MHz, i.e. the Q of the filter is nearly 1.338 million. Meanwhile, based on the cascaded MZIs structure, the FSR is enlarged to about 1.466 GHz. To further enhance the processing range of the filter, the channelized filter is introduced to the system to achieve a processing range of over 110 GHz. Thanks to the high performance of the signal processor, in the experiment, the four-band bandwidth signals from the L-band to the K-band can be extracted and recovered with clean constellations. With the proposed RF photonic frontend technology, the RF signals from L-to K-band are extracted by the signal processor entirely and down-converted to below 100 MHz successfully, which would decrease the bandwidth requirement of the ADC/DSP greatly.

References

[1] J. L. Hill and D. E. Culler, "Mica: A wireless platform for deeply embedded networks," *IEEE Micro*, vol. 22, no. 6, pp. 12–24, Nov. 2002.
[2] G. Frantz, "Digital signal processor trends," *IEEE Micro*, vol. 20, vol. 6, pp. 52–59, Nov./Dec. 2000.
[3] M. G. Taylor, "Coherent detection method using DSP for demodulation of signal and subsequent equalization of propagation impairments," *IEEE Photon. Technol. Lett.*, vol. 16, no. 2, pp. 674–676, Feb. 2004.
[4] M. G. Taylor, "Phase estimation methods for optical coherent detection using digital signal processing," *J. Lightw. Technol.*, vol. 27, no. 7, pp. 901–914, Apr. 2009.
[5] J. Mitola, "Cognitive Radio, an Integrated Agent Architecture for Software Defined Radio," Ph.D. dissertation, Dept. Teleinformatics, Royal Inst. Technol., Stockholm, Sweden, May 2000.
[6] A. A. Abidi, "Evolution of a software-defined radio receiver's RF frontend," in *Proc. IEEE RFIC Dig.*, San Francisco, CA, USA, 2006, pp. 17–20.
[7] R. Bagheri *et al.,* "An 800-MHz–6-GHz software-defined wireless receiver in 90-nm CMOS," *IEEE J. Solid-State Circuits*, vol. 41, vol. 12, pp. 2860–2876, Dec. 2006.
[8] S. Grossman, "Software-defined radio poses major challenges for hardware and software developers," RF Design, Jun. 2005, pp. 10–15. [Online]. Available: www.rfdesign.com
[9] R. Schiphorst, F. Hoeksema, and C. Slump, "The front end of software-defined radio: Possibilities and challenges," in *Proc. Annual CTIT Workshop Mobile Commun.*, 2001, pp. 97–100.

[10] R. Walden, "Performance trends for analog to digital converters," *IEEE Commun. Mag.*, vol. 37, vol. 2, pp. 96–101, Feb. 1999.
[11] F. Rivet *et al.,* "The experimental demonstration of a SASP-based full software radio receiver," *IEEE J. Solid-State Circuits*, vol. 45, vol. 5, pp. 979–988, May 2010.
[12] F. Rivet *et al.,* "From software-defined to software radio: Analog signal processor features," in *Proc. IEEE RWS*, 2009, pp. 348–351.
[13] X. Liu, R. M. Osgood, Y. A. Vlasov, and W. M. Green, "Mid-infrared optical parametric amplifier using silicon nano-photonic waveguides," *Nature Photon.*, vol. 4, pp. 557–560, 2010.
[14] D. J. Blumenthal, P. R. Prucnal, and J. R. Sauer, "Photonic packet switches: Architectures and experimental implementations," *Proc. IEEE*, vol. 82, no. 11, pp. 1650–1667, Nov. 1994.
[15] D. Cotter *et al.,* "Nonlinear optics for high-speed digital information processing," *Science*, vol. 286, no. 5444, pp. 1523–1528, 1999.
[16] J. Capmany and D. Novak, "Microwave photonics combines two worlds," *Nature Photon.*, vol. 1, pp. 319–330, 2007.
[17] J. Yao, "Microwave photonics" *J. Lightw. Technol.*, vol. 27, no. 3, pp. 314–335, Feb. 2009.
[18] D. Marpaung *et al.,* "Integrated microwave photonics," *Laser Photon. Rev.*, vol. 7, no. 4, pp. 506–538, Jul. 2013.
[19] P. Toliver *et al.,* "A programmable optical filter unit cell element for high resolution RF signal processing in silicon photonics," presented at the Opt. Fiber Commun. Conf., San Diego, CA, USA, Mar. 21–23, 2010, Paper OWJ4.
[20] P. Dong *et al.,* "GHz-bandwidth optical filters based on high-order silicon ring resonators," *Opt. Exp.*, vol. 18, no. 23, pp. 23784–23789, Nov. 2010.
[21] S. S. Djordjevic *et al.,* "Fully reconfigurable silicon photonic lattice filters with four cascaded unit cells," *IEEE Photon. Technol. Lett.*, vol. 23, no. 1, pp. 42–44, Jan. 2011.
[22] E. Norberg, R. Guzzon, J. S. Parker, L. A. Johansson, and L. A. Coldren, "Programmable photonic microwave filters monolithically integrated in InP-InGaAsP," *J. Lightw. Technol.*, vol. 29, no. 11, pp. 1611–1619, Jun. 2011.
[23] H. Yu *et al.,* "Silicon-on-insulator narrow-passband filterbased on cascaded MZIs incorporating enhanced FSR for downconverting analog photonic links," *Opt. Exp.*, vol. 21, no. 6, pp. 6749–6755, Mar. 2013.
[24] S. Parkvall, A. Furuskar, and E. Dahlman, "Evolution of LTE toward IMT-advanced," *IEEE Commun. Mag.*, vol. 49, no. 2, pp. 84–91, Feb. 2011.
[25] S. Chen, Y. Wang, W. Ma, and J. Chen, "Technical innovations promoting standard evolution: From TD-SCDMA to TD-LTE and beyond," *IEEE Wireless Commun.*, vol. 19, no. 1, pp. 60–66, Feb. 2012.
[26] F. Morichetti *et al.,* "Box-shaped dielectric waveguides: A new concept in integrated optics?" *J. Lightw. Technol.*, vol. 25, no. 7, pp. 2579–2589, 2007.
[27] L. Zhuang *et al.,* "Low-loss, high-index-contrast Si_3N_4/SiO_2 optical waveguides for optical delay lines in microwave photonics signal processing," *Opt. Exp.*, vol. 19, no. 23, pp. 23 162–23 170, 2011.
[28] L. Zhuang *et al.,* "Integrated photonic signal processors for microwave photonics and optical communications: A progress review in TriPleX™ Si_3N_4 waveguide technology," presented at the Asia Commun. Photonics Conf., Shanghai, China, Nov. 11–14, 2014, Paper ATh1F-3.
[29] C. K. Madsen and J. H. Zhao, *Optical Filter Design and Analysis*. Hoboken, NJ, USA: Wiley-Interscience, 1999, pp. 168–171.
[30] H. Yu, M. Chen, S. Yang, H. Chen, and S. Xie, "All-optical analog programmable signal processor," presented at the Conf. Lasers and Electro-Optics, San Jose, CA, USA, May 10–15, 2015, Paper STu1F.2.